

Maximizing the opening of eye diagrams for slow-light systems

Ravi Pant,^{1,*} Michael D. Stenner,^{1,2} Mark A. Neifeld,^{1,2} Zhimin Shi,³
Robert W. Boyd,³ and Daniel J. Gauthier⁴

¹College of Optical Sciences, University of Arizona, Tucson, Arizona 85721, USA

²Department of Electrical and Computer Engineering, University of Arizona, Tucson, Arizona 85721, USA

³Institute of Optics, University of Rochester, Rochester, New York 14627, USA

⁴Department of Physics and the Fitzpatrick Center for Photonics and Communication Systems, Duke University, Durham, North Carolina 27708, USA

*Corresponding author: rpant@email.arizona.edu

Received 23 February 2007; revised 8 May 2007; accepted 20 July 2007;
posted 24 July 2007 (Doc. ID 80350); published 5 September 2007

We present a data-fidelity metric for quantifying distortion in slow-light optical pulse delay devices. We demonstrate the utility of this metric by applying it to the performance optimization of gain-based slow-light delay systems for Gaussian and super-Gaussian pulses. Symmetric Lorentzian double-line and triple-line gain systems are optimized and achieve maximum delay of 1.5 and 1.7 times the single-line gain system delay, respectively. The resulting double-line gain system design is qualitatively similar to the double-line gain system designed with a previous metric, but is tuned specifically to constrain data fidelity. © 2007 Optical Society of America

OCIS codes: 060.2330, 290.5900.

1. Introduction

Applications such as high-speed optical networking, information processing, and computing can all benefit from all-optical signal processing. Two important functionalities are optical buffering and bit synchronization, both of which require controlled generation of pulse delays relative to the pulse width [1–11]. In recent years, a number of methods have been proposed for slowing light pulses [12–16]. All of these methods exhibit a trade-off between delay-bandwidth product and pulse distortion: pulse distortion increases as the delay-bandwidth product increases. By pulse distortion, we simply mean a change in the pulse shape, including broadening or contraction. Consideration of this delay-distortion trade-off is essential for the design of robust communications systems [17–21].

Recently, Stenner *et al.* proposed a metric to quantify distortion in slow-light-based systems [22]. Their

frequency-domain metric quantifies distortion by considering the device response over a finite bandwidth that is comparable to the pulse bandwidth rather than just at the carrier frequency. Although convenient and conceptually simple, that metric is not directly connected to data fidelity or temporal pulse shape.

In this paper, we present an improved metric that quantifies pulse distortion for slow-light optical pulse delay devices. This metric is based on the eye diagram, which is frequently used to characterize the performance of communication systems and is directly related to pulse detection and digital data fidelity. Using this metric we optimize three different gain-based systems: single, double, and triple Lorentzian lines. We optimize each of these media using two different pulse shapes: Gaussian and super-Gaussian.

A. Distortion Metric

Any pulse propagating through a realistic slow-light medium experiences distortion. These changes in the pulse shape can make reliable pulse detection difficult. In this section, we present our metric to quantify

this distortion and apply it to a single-line gain system using two different pulse shapes.

For each pulse shape, we define the bit period T_0 as the time required to transmit a logical “1” or a logical “0”. In our study, we use a return-to-zero (RZ) modulation scheme for which logical 0 is represented by the absence of a pulse and logical 1 is represented by a pulse that occupies half of the bit period. Using this definition of bit period, we define the pulse amplitudes for RZ Gaussian and super-Gaussian pulses as

$$E_g(t) = \exp\left(-\frac{t^2}{\tau^2}\right), \quad (1)$$

$$E_{sg}(t) = \exp\left(-\frac{t^n}{\tau^n}\right), \quad n > 2, \quad (2)$$

respectively, where $\tau = T_0/4$ is the pulse half-width at $1/e$ amplitude and $1/e^2$ intensity. The Gaussian pulse has a power spectrum given by $S(\omega) \propto \exp(-\omega^2\tau^2/2)$ with a half-width at half-maximum (HWHM) of $\Delta_g = \sqrt{2 \ln(2)}/\tau$. We consider super-Gaussian pulses with $n = 6$. The super-Gaussian power spectrum cannot be so cleanly represented, but it has an HWHM of $\Delta_{sg} \approx 1.2\Delta_g$. For all figures herein, quantities are plotted versus the linewidth-normalized bit rate $B_N = \pi/(T_0\gamma)$. Here, γ is the HWHM of the Lorentzian gain lines used to construct our slow-light systems.

Although Gaussian pulses are rarely used in communication systems, we consider them here because many of the studies of slow-light systems so far have used Gaussian pulses. Super-Gaussian pulses are well contained within the time interval $T_0/2$; whereas, Gaussian pulses extend beyond this period, as shown in Figs. 1(b) and 1(a), respectively. Super-Gaussian pulses, therefore, provide a good approximation of the “square” pulses used in common systems that implement RZ. In practice, pulses from modulated lasers are not perfectly rectangular and have smooth edges. These pulses can be modeled using the super-Gaussian pulses [23]. Moreover, the use of two different pulse shapes demonstrates that this metric applies to different pulse shapes and leads to qualitatively similar medium designs.

Figures 1(a) and 1(b) show Gaussian and super-Gaussian ($n = 6$) pulses, respectively, after propaga-

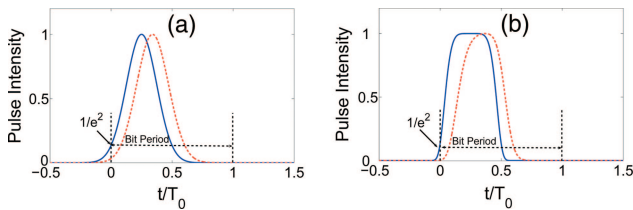


Fig. 1. (Color online) Input (solid curve) and output (dashed curve) (a) Gaussian pulse and (b) super-Gaussian pulse after propagation through a single-line gain system with gain exponent $g_0L = 10$ and $B_N = 0.058$. This bit rate is chosen to demonstrate visible distortion even at small B_N .

tion through a single Lorentzian gain-line system described by the transfer function

$$T_1(\omega) = \exp\left[j\left(\frac{\omega}{c} + \frac{g_0\gamma}{2(\omega - \omega_0 + j\gamma)}\right)L\right], \quad (3)$$

where ω_0 is the optical carrier frequency, g_0 is the gain coefficient, L is the length of the medium, and c is the speed of light in vacuum. The transfer function approach used here to propagate the pulses assumes that the system is linear in the signal field. For small signal field and $g_0L \leq 10$, the transfer function approach and coupled wave theory yield the same results [24]. The coupled wave equations for the pump, signal, and acoustic field, under the slowly varying envelop approximation (SVEA), are given as [24]

$$-\frac{\partial E_p}{\partial z} + \frac{n_{fg}}{c} \frac{\partial E_p}{\partial t} = \frac{-\alpha E_p}{2} + jg_2 E_s \rho, \quad (4)$$

$$\frac{\partial E_s}{\partial z} + \frac{n_{fg}}{c} \frac{\partial E_s}{\partial t} = \frac{-\alpha E_s}{2} + jg_2 E_p \rho^*, \quad (5)$$

$$\frac{\partial \rho}{\partial t} + (\gamma - j\Delta\omega)\rho = \frac{jg_1 E_p E_s^*}{\eta}, \quad (6)$$

where the pump, signal, and acoustic fields are denoted by E_p , E_s , and ρ ; α is the absorption coefficient; n_{fg} is the group index of the fiber mode; $g_1 = \gamma_e \epsilon_0 \Omega_B / (4\nu_a^2)$; $g_2 = \gamma_e \omega_{p0} / (4cn_p \rho_0)$; $\eta = (c\epsilon_0 n_f) / 2$; γ_e is the electrostriction coefficient of the fiber; ϵ_0 is the vacuum permittivity; ν_a is the speed of the acoustic wave; n_f is the modal index of the fiber mode; $\Delta\omega = \omega_0 - \omega_{s0}$ is the detuning from the gain-line center; and ρ_0 is the material density. Under the conditions of undepleted pump and weak signal, transforming Eqs. (4)–(6) to the frequency domain gives

$$\frac{\partial E_s}{\partial z} - j(\omega - \omega_{s0}) \frac{n_{fg} E_s}{c} = jg_2 E_p \rho^*, \quad (7)$$

$$[\gamma - j(\omega - \omega_0)]\rho^* = -j \frac{g_1}{\eta} E_p^* E_s. \quad (8)$$

Here, we have neglected the fiber attenuation ($\alpha = 0$). Substituting ρ^* from Eq. (8) into Eq. (7) one can rewrite the evolution of the signal field E_s as

$$\frac{\partial E_s}{\partial z} = jk(\omega) E_s, \quad (9)$$

where $k(\omega) = n_f \omega / c + (\alpha_0 I_p \gamma) / (\omega - \omega_0 + j\gamma)$; $\alpha_0 = 2g_1 g_2 / (\eta \gamma)$. From Eq. (9) one can see that under the weak signal and undepleted pump approximation, propagation of the signal field can be described by the transfer function approach. To ensure that the system remains linear in the signal field, we restrict the

gain to $g_0L \leq 10$, which earlier experimental results suggest is a reasonable constraint [10]. Recently, Zhu *et al.* demonstrated Brillouin gain slow-light using a broadband pump and 2 km long fiber [3]. The experimental results are shown to be in good agreement with the results using the transfer function approach. Thus, the transfer function approach is also valid for broadband pumps and long fiber as long as the previously mentioned criteria are met. The propagated Gaussian and super-Gaussian pulses are shown in Figs. 1(a) and 1(b). The Gaussian pulse looks slightly broadened with otherwise little change in pulse shape, whereas the super-Gaussian pulse experiences significant distortion, visible primarily as a smoothing of the rising and falling edges.

Although the pulse shown in Fig. 1(b) is visibly distorted, it may still be reliably detected by observing near its peak. For threshold detection, we can quantify the optimal time to detect pulses by using an eye diagram. For a sequence of pulses, an eye diagram is created by superimposing the pulses corresponding to 0s and 1s over a fixed time interval. Figure 2 shows an eye diagram for a random pulse sequence of 0s and 1s before and after propagation through a single-line gain system. The eye diagram degrades after propagation through the medium, as shown in Fig. 2(b). The degradation in the eye diagram can be quantified using standard metrics such as eye opening, power penalty, etc. [25–29]. The choice of metric may vary from application to application. Although the output eye diagram looks different from the input eye diagram, the output pulses can still be reliably detected by observing the pulses at the moment when the eye opening is maximum. Eye opening E is defined as the difference between the minimum of the 1s and the maximum of the 0s. The eye opening determines the amount of noise that can be tolerated; a larger eye opening is better as it reduces the error probability in detection of 0s and 1s. Herein, we have normalized all the eye diagrams so that the maximum eye opening varies from 0 to 1. This normalization corresponds to a physical attenuation of the signal after propagation through a gain medium to preserve the desired power level at the detector input. After normalization, a fixed amount of noise is added to the pulses, corresponding to the detector-noise-limited case. In this way, the signal-to-noise ratio (SNR) remains fixed. The optimal time to detect a pulse is the time when the eye opening is

maximum. Pulse delay can therefore be defined as the time difference between the maximum eye openings of the output and input eye diagrams.

Based on the eye diagram, we define distortion D as

$$D = 1 - \max(E). \quad (10)$$

Ideal noiseless input pulses will lead to $\max(E) = 1$ and $D = 0$. In the case of noisy input, $D > 0$ indicates that the input is itself corrupted. After propagation through the medium, changes to the pulse shape and additional noise will reduce the eye opening and further increase D . In this sense, D quantifies more than just pulse distortion, but limiting D does limit the impact on data fidelity from pulse distortion. In our study, we are considering detector-limited-noise and so $D = 0$ for input pulses and at the output of the pulse delay medium D therefore quantifies only the effect of the medium. The distortion measure D can be related to data fidelity by considering the relationship between eye opening, Q factor, and bit error rate (BER). The Q factor is defined as $Q = (P_1 - P_0)/(\sigma_1 + \sigma_0)$, where P_1 and P_0 are the minimum of 1 and maximum of 0 at the maximum eye opening instant [29]; σ_1 and σ_0 are the noise standard deviations for levels 1 and 0, respectively. The BER is then given by $BER = (1/2)\text{erfc}(Q/\sqrt{2})$. This relationship between distortion D and BER depends on the noise level. For all of the following results, we maintain a detector-noise-limited SNR of 35 dB at the receiver. Given this SNR, we chose a distortion constraint $D \leq 0.35$ so that the inter-symbol interference (ISI) is small and BER is less than 10^{-12} . Note that power penalty (PP), another common metric for characterizing optical components, is monotonically related to distortion according to

$$PP = 10 \log_{10} \left(\frac{1 + r_{ex}}{1 - r_{ex}} \right), \quad (11)$$

where $r_{ex} = P_0/P_1$ [28,29]. Thus, as the eye opening $E = P_1 - P_0$ decreases, both distortion D and power penalty increase.

To demonstrate the use of this metric, we use it to characterize the performance of a single-line gain system described by Eq. (3). We characterize the delay-distortion performance of this single-line gain system by studying the variation of D and the fractional pulse delay $\Delta T/T_{\text{pulse}}$ ($T_{\text{pulse}} = T_0/2$) as functions of bit rate B_N . The maximum intensity gain exponent g_0L is constrained such that $g_0L \leq 10$. The maximum value of the gain exponent depends on factors such as pump power limits, the system threshold for nonlinear optical effects, noise, etc. Therefore, the maximum usable gain will vary from one slow-light system to another. In this study, we simulate a stimulated-Brillouin-scattering (SBS) slow-light medium consisting of 1 km of fiber and Brillouin shifted pump and probe lasers. The probe is modulated using an external Mach–Zehnder modulator and the pump

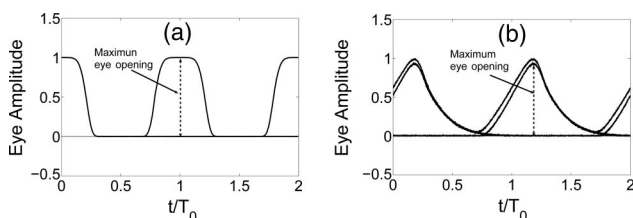


Fig. 2. Eye diagram for (a) input data stream and (b) output data stream after propagation through a single-line gain system with gain exponent $g_0L = 4.0$ and $B_N = 0.42$.

power is controlled using the erbium-doped fiber amplifier gain module. For double-line and triple-line gain systems (see Section 2), the pump can be modulated using a Mach–Zehnder modulator to generate the doublet sidebands. The frequency separation between the doublet lines (as described in Section 2) is tuned by varying the modulation frequency. Based on this choice of system, we choose a maximum g_0L value of 10, which is reasonable for Brillouin gain systems [10].

The results of characterizing this single-line SBS system are shown in Fig. 3. Figures 3(a) and 3(b) show the fractional pulse delay and distortion, respectively, for a random Gaussian pulse sequence and fixed $g_0L = 10$. For fixed g_0L , fractional pulse delay $\Delta T/T_{\text{pulse}}$ increases as we decrease T_{pulse} , i.e., increase the bit rate. This increase in the fractional pulse delay with the bit rate comes at the cost of greater distortion. At a normalized bit rate of 0.43 the distortion limit is reached. Increasing the bit rate beyond 0.43 causes the system to exceed the distortion limit. This implies that a fractional pulse delay of ≈ 1 is the largest possible under the distortion constraint at $g_0L = 10$. This example demonstrates that one cannot simply employ the maximum gain at high bit rates because the distortion will become unacceptably large.

To maximize the fractional pulse delay at each bit rate while simultaneously limiting distortion, one must optimize the system parameters as described in Section 2. In the case of a single-line gain system, there is only one free parameter: the gain. Therefore, at each bit rate, we maximize the fractional pulse delay by varying g_0L subject to the constraints $g_0L \leq 10$ and $D \leq 0.35$. Figure 4 shows the results of this single-line gain system optimization.

Figure 4(a) indicates that the largest fractional pulse delay occurs when both the gain and distortion constraints are met simultaneously. This condition occurs at a normalized bit rate of 0.43. To the left of this point (smaller bit rate) the system is gain-limited, and to the right (larger bit rate) it is distortion-limited, as shown in Figs. 4(b) and 4(c). This implies that at larger bit rates, keeping the gain fixed at its maximum value leads to unacceptable distortion, and therefore the gain parameter must reduce to satisfy the distortion constraint. This is effectively a sacrifice in pulse delay, but a necessary one if we insist on reliable data detection.

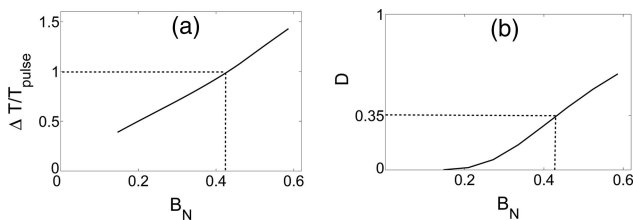


Fig. 3. Variation of (a) fractional delay and (b) resulting distortion with fractional bit rate for a single-line gain system. Results are obtained for $g_0L = 10$.

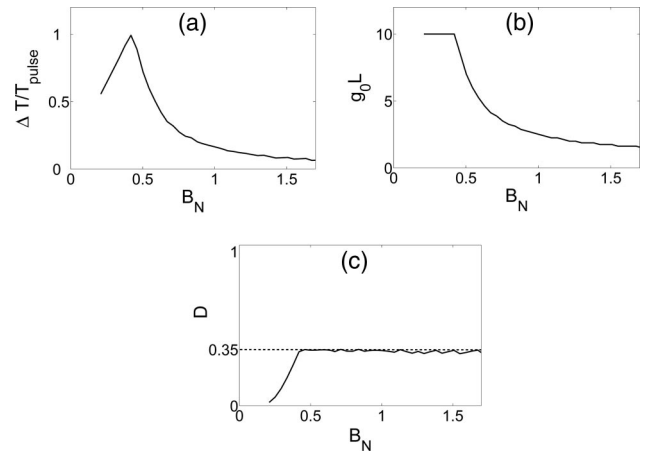


Fig. 4. (a) Optimized fractional delay plotted against normalized bit rate B_N for a single-line gain system subject to the distortion constraint $D \leq 0.35$ and the gain constraint $g_0L \leq 10$. That the maximum delay is approximately 1 is purely coincidental and depends on the values of the gain and distortion constraints as well as the pulse shape. (b) Corresponding value of the gain exponent g_0L and (c) distortion D of the transmitted pulse.

For optimizing the system parameters, we perform an adaptive search over the parameter space for each bit rate and choose the parameters that maximize the fractional pulse delay under the distortion constraint $D \leq 0.35$. The optimization begins with a search using a coarse grid of parameters. The grid spacing is then refined iteratively in the neighborhood of the best solution. The search ends when $D \approx 0.35$ and the best fractional delay changes by less than 2%. Because this search has finite granularity, the best observed parameters that satisfy the constraint inequalities differ slightly from the ideal parameters. This is visible especially at higher bit rates, where D is more sensitive to small gain fluctuations.

The delay performance of a single-line gain system can be improved by using multiple gain lines [22]. In Section 2, we will use multiple gain lines to improve the delay performance at higher bit rates using this new metric.

2. Distortion Compensation Using Multiple Gain Lines

For single-line gain systems, we observe that gain and distortion constraints limit the maximum achievable fractional delay. While this is true for any system, choosing a system with additional degrees of freedom can improve the maximum delay [22,30]. Recall that the single-line gain system had only one free parameter: the gain. For multiple-line gain systems, the number of degrees of freedom increases. In this study, we consider double-line and triple-line gain systems, characterized by the transfer functions

$$T_2(\omega) = \exp \left[j \left(\frac{\omega}{c} + \frac{g\gamma}{2((\omega - \omega_0 - \delta) + j\gamma)} + \frac{g\gamma}{2((\omega - \omega_0 + \delta) + j\gamma)} \right) L \right], \quad (12)$$

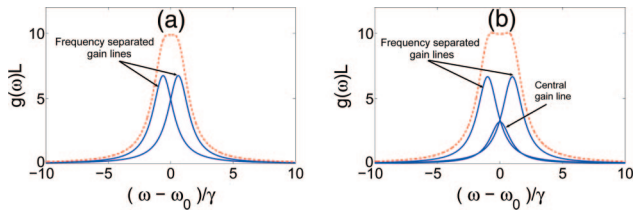


Fig. 5. (Color online) Gain versus detuning from carrier frequency for (a) example double-line gain system with $gL = 6.75$ and $\delta/\gamma = 0.67$ and (b) example triple-line gain system with $g_0L = 3.2$, $gL = 6.67$, and $\delta/\gamma = 0.99$. In each case, the dotted curve shows the net gain exponent and the solid curves show the constituent Lorentzian lines.

$$T_3(\omega) = \exp \left[j \left(\frac{\omega}{c} + \frac{g\gamma}{2((\omega - \omega_0 - \delta) + j\gamma)} + \frac{g_0\gamma}{2((\omega - \omega_0) + j\gamma)} + \frac{g\gamma}{2((\omega - \omega_0 + \delta) + j\gamma)} \right) L \right], \quad (13)$$

respectively, where g_0 is the gain coefficient of the central gain line for the triple-line gain system, g is the gain coefficient of the separated gain lines for both the double-line and triple-line gain systems, 2δ is the frequency separation between the separated lines, and γ is the HWHM of all Lorentzian gain lines.

Figures 5(a) and 5(b) show the component and overall gain spectra for the double-line and triple-line gain systems, respectively. Use of multiple gain lines makes the gain uniform over a larger bandwidth compared to the single-line gain system, and thus increases the distortion-limited bandwidth. This suggests that the maximum gain can be extended over a larger fractional bandwidth than in the single-line gain system, resulting in increased fractional delay. This slow-light gain-flattening was recently studied analytically by Khurgin, who showed that the delay performance of optical amplifiers can be improved, but the gain required for achieving a fractional delay N_{st} varies as $N_{st}^{3/2}$ even with gain flattening [31]. It is also possible to generate a broad, flat gain spectrum using a continuously broadened pump [3–6].

For double-line and triple-line gain systems, we optimize the system parameters at each normalized bit rate B_N to maximize the delay as we did for the single-line gain system. Figures 6(a) and 7(a) show the fractional delay for single-line, double-line, and triple-line gain systems optimized for super-Gaussian and Gaussian pulses, respectively. For the double-line gain system, we optimize g and δ , whereas for the triple-line gain system we optimize g_0 , g , and δ . In all cases the distortion is limited to $D \leq 0.35$, and the maximum gain at any frequency ω is limited to 10.

For normalized bit rates smaller than 0.43, the optimal fractional delay achieved for single-line, double-line, and triple-line gain systems is identical. In this region, the additional degrees of freedom are not required because the distortion limit has not been

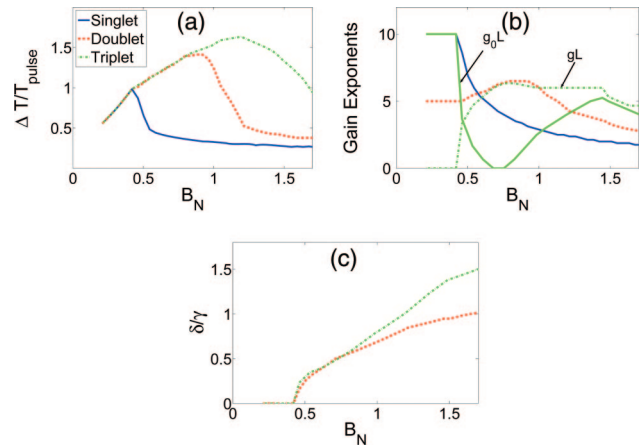


Fig. 6. (Color online) Comparison of (a) optimized fractional delay, (b) optimized gain exponent, and (c) optimized frequency separation for super-Gaussian data sequences for three gain systems.

reached, and maximum gain is achieved by a single-line gain system. Therefore, the double-line and triple-line gain systems mimic a single-line gain system. For the double-line gain system, when ($B_N \leq 0.43$), the linewidth-normalized frequency separation (δ/γ) is zero [Figs. 6(c) and 7(c)] and the gain exponent for each line is half of the maximum value [Figs. 6(b) and 7(b)]. For the triple-line gain system, only the central gain line contributes ($g = 0$), and it has the maximum gain, $g_0L \approx 10$.

For larger bit rates, the single-line gain system reaches the distortion limit, and the gain must be reduced to maintain acceptable distortion. This results in a decrease in delay for the single-line gain system. However, at this point, the double-line and triple-line gain systems begin to use their additional degrees of freedom. In the bit rate region from 0.43 to 0.94, the double-line and triple-line gain systems simultaneously achieve maximum gain and distortion by acting as an optimally spaced double-line gain system. Specifically, we note that the gain of the cen-

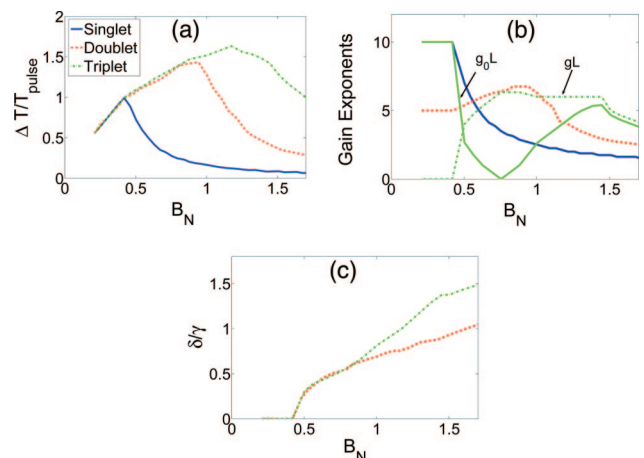


Fig. 7. (Color online) Comparison of (a) optimized fractional delay, (b) optimized gain exponent, and (c) optimized frequency separation for Gaussian data sequences for three gain systems.

tral line of the triple-line gain system reduces making the double-line and triple-line gain systems nearly identical. At a bit rate of 0.94, the double-line gain system can no longer maintain the maximum gain without excessive distortion, and so it must reduce its gain as the single-line gain system did before. However, at this bit rate, the central line gain g_0 of the triple-line gain system continues to increase, and the frequency separation increases further to maintain the maximum gain. It continues to produce increasing delay until a bit rate of 1.17, when it too must reduce its gain to avoid excessive distortion.

The overall result of this optimization is that double-line and triple-line gain systems achieve significantly larger distortion-constrained fractional delay compared to the single-line gain system. Using a double-line gain system improves the fractional delay performance by factors of 4 and 7 for super-Gaussian and Gaussian pulses, respectively, compared to a single-line gain system at the same bit rate ($B_N \approx 0.94$). We also note that for both pulse shapes the double-line gain system provides 1.5 times the best single-line gain system delay. For a Gaussian pulse stream, the triple-line gain system improves the fractional delay performance by a factor of 12 and 2 compared to single-line and double-line gain systems, respectively, at the same bit rate ($B_N \approx 1.17$). For super-Gaussian pulses, these improvement factors are 5.5 and 2.5, respectively. At higher bit rates, the pulse edges are smoothed by the comparatively narrow gain line. As a result, the peak of the output pulse and moment of maximal eye opening shifts toward the trailing edge of pulse. This leads to a measured delay ΔT slightly less than $T_{\text{pulse}}/2$, as shown in Fig. 6(a). The optimum triple-line gain system fractional delay is also 1.7 and 1.15 times better than the best single-line and double-line gain system delays, respectively. These improvement factors are observed for both Gaussian and super-Gaussian pulses. Table 1 summarizes the delay and bandwidth values for the single-, double-, and triple-line gain system. The Brillouin gain linewidth in optical fibers is ~ 50 MHz full width at half-maximum (FWHM). Note that the double-line and triple-line gain system extend the optimal gain spectral width 2 and 2.7 times the single-line gain system, respectively. Using a broadband pump (whether discrete or continuous), the gain bandwidth can be extended arbitrarily to design high data-rate systems [3–6].

The optimization results obtained with this metric show trends similar to the previously reported results for single-line and double-line gain systems [22] and recent results from Shi *et al.* and Minardo *et al.* for double-line and triple-line gain systems using a

transfer-function metric [32,33]. The advantage of working with our metric is that it deals directly with the pulses and, being based on eye opening, directly reflects the reliability of received data. Although the maximum achieved fractional delay of 1.7 pulse width observed in our study is not practical for optical buffering, this delay can be easily tuned by adjusting the gain. Tunable delay of one pulse width is very useful for data synchronization [18]. Furthermore, this method of combining multiple delay elements based on data fidelity can be used to achieve comparable improvement with other delay techniques such as coupled resonators [13] or electromagnetically induced transparency [34,35].

3. Conclusion

We have presented a data-fidelity metric for slow-light systems based on eye diagrams. Our results are qualitatively similar to those obtained with transfer-function-based metrics. The qualitative similarity supports the usefulness of those metrics, although the approach described herein is more directly connected to data fidelity. We observe fractional delay improvement factors of 7 and 12 using double-line and triple-line gain systems, compared to a single-line gain system at the same bit rate.

We gratefully acknowledge the financial support of the DARPA DSO Slow-Light Program. We would also like to thank Alan E. Wilner for his helpful input and discussion.

References

1. F. G. Sedgwick, B. Pesala, J. Y. Lin, W. S. Ko, X. Zhao, and C. J. Chang-Hasnain, "THz-bandwidth tunable slow light in semiconductor optical amplifiers," *Opt. Express* **15**, 747–753 (2007).
2. E. Shumakher, A. Willinger, R. Blit, D. Dahan, and G. Eisenstein, "Large tunable delay with low distortion of 10 Gbit/s data in a slow-light system based on narrowband fiber parametric amplification," *Opt. Express* **14**, 8540–8545 (2006).
3. Z. Zhu, A. M. C. Dawes, D. J. Gauthier, L. Zhang, and A. E. Willner, "Broadband SBS slow light in optical fibers," *J. Light-wave Technol.* **25**, 201–206 (2007).
4. M. G. Herráez, K. Y. Song, and L. Thévenaz, "Arbitrary-bandwidth Brillouin slow light in optical fibers," *Opt. Express* **14**, 1395–1400 (2006).
5. A. Zadok, A. Eyal, and M. Tur, "Extended delay of broadband signals in stimulated Brillouin scattering slow light using synthesized pump chirp," *Opt. Express* **14**, 8498–8505 (2006).
6. S. Chin, M. G. Herráez, and L. Thévenaz, "Zero-gain slow- and fast-light propagation in an optical fiber," *Opt. Express* **14**, 10684–10692 (2006).
7. S. Blair and K. Zheng, "Intensity-tunable group delay using stimulated Raman scattering in silicon slow-light waveguides," *Opt. Express* **14**, 1064–1069 (2006).
8. Q. Sun, Y. V. Rostovtsev, J. P. Dowling, M. O. Scully, and M. S. Zhubairy, "Optically controlled delays for broadband pulses," *Phys. Rev. A* **72**, 031802 (2005).
9. K. Y. Song, M. G. Herráez, and L. Thévenaz, "Long optically controlled delays in optical fibers," *Opt. Lett.* **30**, 1782–1784 (2005).
10. Y. Okawachi, M. S. Bigelow, J. E. Sharping, Z. M. Zhu, A. Schweinsberg, D. J. Gauthier, R. W. Boyd, and A. L. Gaeta, "Tunable all-optical delays via Brillouin slow light in an optical fiber," *Phys. Rev. Lett.* **94**, 153902 (2005).

Table 1. Maximum Fractional Delay and Respective Pulse Bandwidth

| Medium | ΔT_{max} (ns) | $BW_{\text{pulse}} = 1/T_{\text{pulse}}$ (MHz) |
|-------------|------------------------------|--|
| Single-line | 22.3 | 43 |
| Double-line | 15.3 | 94 |
| Triple-line | 14.1 | 117 |

11. Y. A. Vlasov, M. O'Boyle, H. F. Hamann, and S. J. McNab, "Active control of slow light on a chip with photonic crystal waveguides," *Nature* **438**, 65–69 (2005).
12. L. V. Hau, S. E. Harris, Z. Dutton, and C. H. Behroozi, "Light speed reduction to 17 meters per second in an ultracold atomic gas," *Nature* **397**, 594–598 (1999).
13. J. E. Heebner and R. W. Boyd, "Slow and fast light in resonator-coupled waveguides," *J. Mod. Opt.* **49**, 2629–2636 (2002).
14. M. S. Bigelow, N. N. Lepeshkin, and R. W. Boyd, "Superluminal and slow-light propagation in a room-temperature solid," *Science* **301**, 200–202 (2003).
15. D. Mori and T. Baba, "Dispersion-controlled optical group delay device by chirped photonic crystal waveguides," *Appl. Phys. Lett.* **85**, 1101–1103 (2004).
16. R. S. Tucker, P. C. Ku, and C. J. Chang–Hasnain, "Delay-bandwidth product and storage density in slow-light optical buffers," *Electron. Lett.* **41**, 208–209 (2005).
17. R. W. Boyd and D. J. Gauthier, in *Progress in Optics*, E. Wolf, ed. (Elsevier, 2002), Chap. 6, pp. 497–530.
18. D. Gauthier, "Slow light brings faster communication," *Phys. World* **18**, 30–32 (2005).
19. D. J. Gauthier, A. L. Gaeta, and R. W. Boyd, "Slow light: from basics to future prospects," *Photonics Spectra*, March 2006, pp. 44–50.
20. R. W. Boyd, D. J. Gauthier, and A. L. Gaeta, "Applications of slow light in telecommunications," *Opt. Photon. News* **17**(4), 18–23 (2006).
21. R. W. Boyd, D. J. Gauthier, A. L. Gaeta, and A. E. Wilner, "Maximum time delay achievable on propagation through a slow-light medium," *Phys. Rev. Lett.* **71**, 023801 (2005).
22. M. D. Stenner, M. A. Neifeld, Z. Zhu, A. M. C. Dawes, and D. J. Gauthier, "Distortion management in slow-light pulse delay," *Opt. Express* **13**, 9995–10002 (2005).
23. G. P. Agarwal, *Nonlinear Fiber Optics*, 3rd ed. (Academic, 2001), Chap. 3, pp. 72–73.
24. Z. Zhu, D. J. Gauthier, Y. Okawachi, J. E. Sharping, A. L. Gaeta, R. W. Boyd, and A. E. Wilner, "Numerical study of all-optical slow-light delays via stimulated Brillouin scattering in an optical fiber," *J. Opt. Soc. Am. B* **22**, 2378–2384 (2005).
25. E. Shumakher, N. Orbach, A. Nevet, D. Dahan, and G. Eisenstein, "On the balance between delay, bandwidth, and signal distortion in slow-light systems based on stimulated Brillouin scattering in optical fibers," *Opt. Express* **14**, 5877–5884 (2006).
26. J. T. Mok, J. L. Blows, and B. J. Eggleton, "Investigation of group delay ripple distorted signals transmitted through all-optical 2R regenerators," *Opt. Express* **12**, 4411–4422 (2004).
27. F. G. Sedgwick, C. J. Chang–Hasnain, P. C. Ku, and R. S. Tucker, "Storage-bit-rate product in slow-light optical buffers," *Electron. Lett.* **41**, 1347–1348 (2005).
28. M. Kuznetsov, N. M. Froberg, S. C. Henion, and K. A. Rauschenbach, "Power penalty for optical signals due to dispersion slope in WDM filter cascades," *IEEE Photon. Technol. Lett.* **11**, 1411–1413 (1999).
29. J. D. Downie, "Relationship of Q penalty to eye-closure penalty for NRZ and RZ signals with signal-dependent noise," *J. Lightwave Technol.* **23**, 2031–2038 (2005).
30. Z. Lu., Y. Dong, and Q. Li, "Slow light in multi-line Brillouin gain spectrum," *Opt. Express* **15**, 1871–1877 (2007).
31. J. B. Khurgin, "Performance limits of delay lines based on optical amplifiers," *Opt. Lett.* **31**, 948–950 (2006).
32. Z. Shi, R. W. Boyd, Z. Zhu, D. J. Gauthier, R. Pant, M. D. Stenner, and M. A. Neifeld, "Distortion-reduced pulse-train propagation with large delay in a triple gain media," in *OSA Slow and Fast Light Conference* (OSA, 2006).
33. A. Minardo, R. Bernini, and L. Zeni, "Low distortion Brillouin slow light in optical fibers using AM modulation," *Opt. Express* **14**, 5866–5876 (2006).
34. A. Kasapi, M. Jain, G. Y. Yin, and S. E. Harris, "Electromagnetic induced transparency: propagation dynamics," *Phys. Rev. Lett.* **74**, 2447–2451 (1995).
35. B. Macke and B. Segard, "Pulse normalization in slow-light media," *Phys. Rev. A* **73**, 043802 (2006).